JGR Oceans

RESEARCH ARTICLE
10.1029/2020JC016609

The Pacific Equatorial Undercurrent in Three Generations of Global Climate Models and Glider Observations

Kristopher B. Karnauskas[1], Julie Jakoboski[2], T. M. Shaun Johnston[3], W. Brechner Owens[4], Daniel L. Rudnick[3], and Robert E. Todd[4]

[1]Cooperative Institute for Research in Environmental Sciences and Department of Atmospheric and Oceanic Sciences, University of Colorado Boulder, Boulder, CO, USA, [2]MetOcean Solutions, Raglan, New Zealand, [3]Scripps Institution of Oceanography, La Jolla, CA, USA, [4]Department of Physical Oceanography, Woods Hole Oceanographic Institution, Woods Hole, MA, USA

Key Points:
- A recent glider campaign offers a unique opportunity to evaluate model simulations of equatorial circulation in a key region for climate
- Global climate model simulations of the Equatorial Undercurrent have improved, but a slow bias of ~36% remains in the eastern Pacific
- Details of the encounter of the Equatorial Undercurrent with the Galápagos are impactful; resolving them well is demonstrably important

Supporting Information:
- Supporting Information S1

Correspondence to:
K. B. Karnauskas,
kristopher.karnauskas@colorado.edu

Citation:
Karnauskas, K. B., Jakoboski, J., Johnston, T. M. S., Owens, W. B., Rudnick, D. L., & Todd, R. E. (2020). The Pacific Equatorial Undercurrent in three generations of global climate models and glider observations. *Journal of Geophysical Research: Oceans*, *125*, e2020JC016609. https://doi.org/10.1029/2020JC016609

Received 15 JUL 2020
Accepted 2 SEP 2020
Accepted article online 22 OCT 2020

Abstract The Equatorial Undercurrent (EUC) is a vital component of the coupled ocean-atmosphere system in the tropical Pacific. The details of its termination near the Galápagos Islands in the eastern Pacific have an outsized importance to regional circulation and ecosystems. Subject to diverse physical processes, the EUC is also a rigorous benchmark for global climate models (GCMs). Simulations of the EUC in three generations of GCMs are evaluated relative to recent underwater glider observations along 93°W. Simulations of the EUC have improved, but a slow bias of ~36% remains in the eastern Pacific, along with a dependence on resolution. Additionally, the westward surface current is too slow, and stratification is too strong (weak) by ~50% above (within) the EUC. These biases have implications for mixing in the equatorial cold tongue. Downstream lies the Galápagos, now resolved to varying degrees by GCMs. Properly representing the Galápagos is necessary to avoid new biases as the EUC improves.

Plain Language Summary The Equatorial Undercurrent (EUC) is a swift current that flows eastward along the equator in the Pacific Ocean, about 100 m below the surface. This current is just as challenging to observe as it is to simulate with models—after all, it was only discovered in the 1950s. One of the interesting aspects of the Undercurrent is how it is diverted by the Galápagos Islands when it encounters them in the eastern Pacific. The resultant upwelling is responsible for the remarkably productive and diverse ecosystem of the Galápagos. This paper takes advantage of a unique set of observations from a recent, successful field campaign using underwater gliders to measure the Undercurrent just before it reaches the Galápagos, in order to evaluate how the latest generations of global climate models simulate this current and its neighboring features. Models have steadily improved, but they still struggle to capture the high speed of the EUC. Models are also being run at finer spatial resolution, which enables islands like the Galápagos to be included in some of the model grids. A sampling of islands in different models, and how they interact with the EUC, demonstrates the importance of a proper representation of the Galápagos in models.

1. Introduction

The eastern equatorial Pacific Ocean is an important region where variations in sea surface temperature (SST) are the result of a balance between upwelling, mixing, and surface heating and are known to exert an outsized influence on global climate through coupling with the atmosphere (Bjerknes, 1969; Kessler, 2006; Warner & Moum, 2019; Wyrtki, 1975). The Equatorial Undercurrent (EUC) is a key component of the tropical ocean circulation. Shoaling and upwelling as it flows eastward along the equator, the EUC transports cold, nutrient-rich water and releases carbon to the atmosphere (e.g., Bryden & Brady, 1985; Feely et al., 2002; Kessler et al., 1998; Sloyan et al., 2003). The resulting cold tongue reinforces the zonal SST gradient, and processes therein play a vital role in global biogeochemistry (e.g., Feely et al., 2002) and shaping oxygen minimum zones (Busecke et al., 2019; Doney & Karnauskas, 2014). In fully coupled global climate models (GCMs), the EUC is also a useful diagnostic of the coupled system (Cravatte et al., 2007), resulting from a balance between the basin-scale

horizontal pressure gradient and the local, downward penetration of momentum imparted by the wind stress (Johnson & Luther, 1994; Qiao & Weisberg, 1997)—effectively given by the Walker circulation—but also sensitive to a wide range of physical processes and parameterizations including horizontal diffusion (Maes et al., 1997), entrainment (Pedlosky, 1988), vertical mixing (Yu & Schopf, 1997), and eddies (Brown et al., 2007). Finally, adequate simulation of the EUC and its relation to wind forcing in coupled models has recently been shown to be essential for simulating realistic ENSO dynamics and observed asymmetries (Hayashi et al., 2020).

Until very recently, repeat observations of the EUC in the Pacific suitable for model evaluation have been limited mainly to the moorings of the Tropical Atmosphere Ocean (TAO) array (McPhaden et al., 1998) and underway measurements by cruises servicing them (Johnson et al., 2002). Historical observations east of the terminus of the TAO array at 95°W are scarce and ad hoc (Karnauskas et al., 2010), except for the comprehensive hydrographic study by Lukas (1986). This gap in observing the EUC in the eastern Pacific was problematic (Kessler, 2006), particularly because just a few hundred km (3.3° longitude) east of the 95°W TAO line lies the Galápagos Archipelago. Small as the Galápagos may be, its location straddling the equator diverts the EUC and is potentially relevant to multiple systematic GCM biases. Moreover, a range of ocean GCM (OGCM) simulations conducted over the past two decades have predicted that the Galápagos strongly impedes the eastward flow of the EUC and results in locally enhanced upwelling (e.g., Cravatte et al., 2007; Eden & Timmermann, 2004; Karnauskas et al., 2007). This upwelling supplies the nutrients sustaining the famously productive Galápagos ecosystem from plankton to penguins (Feldman et al., 1984; Houvenaghel, 1978). Several studies have shown that this ecosystem along with the EUC may be changing due to anthropogenic radiative forcing (Drenkard & Karnauskas, 2014; Karnauskas & Cohen, 2012; Karnauskas et al., 2016, 2015; Luo et al., 2009). The extent to which GCMs can be used to understand those projections for Galápagos upwelling remains uncertain.

Given the well-known influence of the EUC on the environment and ecosystem of islands near the equator from the Gilberts in the central Pacific (Karnauskas et al., 2012, 2016, 2017) to the Galápagos in the eastern Pacific, its importance in maintaining the mean equatorial circulation, and the potential role of a changing EUC to influence tropical SST trends (Coats & Karnauskas, 2018), it is critical to evaluate this aspect of the equatorial ocean circulation in the eastern Pacific in the latest generation of GCMs. To that end, this study compares the EUC in GCMs to the mean observations from the "Repeat Observations by Gliders in the Equatorial Region" (ROGER) campaign, which used a fleet of autonomous underwater gliders to measure the EUC along 93°W and its subsequent encounter with the Galápagos Archipelago (Jakoboski et al., 2020; Rudnick, Owens, Johnston, et al., 2020). ROGER thus presents a unique opportunity to evaluate GCMs, which was not possible in previous studies of similar nature (Karnauskas et al., 2012). In particular, this study seeks to answer the following questions:

1. How well do GCMs compare to ROGER observations of the EUC (including relevant shear and stratification) in the eastern Pacific, just prior to the EUC encountering the Galápagos Archipelago?
2. Has there been an overall improvement in the simulation of the EUC, broadly but particularly in the eastern Pacific, across the latest three generations of GCMs? As a corollary, has the dependence of EUC bias on ocean model resolution identified in an earlier generation of GCMs (Karnauskas et al., 2012) persisted into the latest generation of GCMs?
3. How does the latest generation of GCMs represent the Galápagos Archipelago, and is there any discernable impact of their islands on the EUC that is comparable to our recent analysis of ROGER observations (Jakoboski et al., 2020)?

The remainder of this paper is organized as follows. The following section describes the GCMs analyzed and how their outputs were processed for analysis and the two observational data sets used for direct comparison with the GCMs. Section 3 begins with a broad view of the EUC across the Pacific with comparison to historical observations and a brief update of the analysis of Karnauskas et al. (2012) focusing on the two generations of GCMs that have since emerged. Section 3 also compares the simulated EUC at 93°W with ROGER observations. A qualitative examination of the encounter of the EUC with the Galápagos in the latest generation of GCMs follows. The final section summarizes the results and places them in the context of future modeling and observing of this sentinel region of the global climate system.

2. Data and Methods

2.1. GCMs

Simulations by a total of 90 GCMs from three consecutive Coupled Model Intercomparison Projects (CMIPs) are analyzed in this study: 21 from CMIP3 (Meehl et al., 2007), 35 from CMIP5 (Taylor et al., 2012), and 34 from CMIP6 (Eyring et al., 2016) (CMIP4 did not exist). These sets of models and their experiments are aligned with the Fourth (AR4), Fifth (AR5), and Sixth (AR6) Assessment Reports of the Intergovernmental Panel on Climate Change (IPCC), respectively. All participating models were included so long as their ocean zonal velocity output fields from historical experiments were provided to the Earth System Grid Federation (ESGF), and the vast majority of models participating in IPCC AR4, AR5, and AR6 did so. In addition, potential temperature and salinity fields were acquired (for CMIP6 models only) to calculate potential density and permit analysis of stratification. The stratification metric used is the buoyancy frequency squared (N^2), defined as

$$N^2 = -\frac{g}{\sigma}\frac{\partial \sigma}{\partial z},$$

where g is gravity and σ is potential density.

Following Karnauskas et al. (2012), monthly means from the 1990s were extracted from each model's historical experiment (labeled "Climate of the Twentieth Century" [20C3M] in CMIP3 and simply "historical" in CMIP5 and CMIP6). A much-reduced and harmonized version of the entire CMIPx ocean zonal velocity (and potential temperature and salinity for CMIP6) output data set was produced by retaining the time-means of 3-D output within the domain 160°E to 80°W, 3°S to 3°N, 0–400 m, and linearly regridding to a common grid (0.25° in longitude, 0.1° in latitude, and 1 m in depth). The resulting analysis set is provided freely (see Data Availability Statement).

2.2. Observations

Two observational data sets are utilized for comparison with GCM fields. For observations of the EUC across the broader equatorial Pacific, we use the Acoustic Doppler Current Profiler (ADCP) climatology of Johnson et al. (2002), which is based on 172 meridional sections taken mostly by TAO maintenance cruises between 1991 and 2000 spanning 10 longitudes between 165°W and 95°W.

For an observational description of the EUC along 93°W (~150 km west of the Galápagos), we use the recent ROGER campaign from October 2013 through October 2016 (Jakoboski et al., 2020; Rudnick, Owens, Johnston, et al., 2020). One of the central goals of ROGER was to quantify the EUC with fine horizontal resolution using Spray underwater gliders equipped with ADCPs (Rudnick, 2016; Rudnick et al., 2004, 2018; Sherman et al., 2001; Todd et al., 2017). Importantly, ROGER extended our knowledge of the EUC east of the TAO array and the Johnson et al. (2002) climatology all the way to its encounter with the Galápagos. The sampling pattern of ROGER formed a nearly closed trapezoid bounded on the west by 93°W from 2°S to 2°N and two diagonal lines connecting 93°W with the northern and southern tips of Isla Isabela in the Galápagos (see Figure 1 of Rudnick, Owens, Johnston, et al., 2020). A goal was to observe the velocity field just west of the Galápagos and to quantify the volume transports around the north and south of Isla Isabela—thus enabling an estimate of divergence and upwelling. Glider occupation on 93°W was reasonably well sustained, with a total of 6,346 dives within 60 km of 93°W (Rudnick, Owens, Johnston, et al., 2020). Absolute velocity estimates from the glider ADCPs are available at 10-m vertical resolution for each glider dive. Here we use the mean zonal velocity field along 93°W estimated from ROGER glider observations by Rudnick, Owens, Johnston, et al. (2020). An upper bound on the estimated error (including measurement and sampling) in this mean zonal velocity is 0.07 m s^{-1} (Rudnick, Owens, Johnston, et al., 2020), which is relatively small compared to the peak velocity of the EUC (~0.5 m s^{-1}) and (as will be shown) small compared to differences between observations and certain sets of GCM simulations. It is important to note that the ROGER campaign coincided with the major 2015–2016 El Niño (Rudnick, Owens, Johnston, et al., 2020), which is well known to produce large anomalies in the EUC and sometimes reducing its flow to approximately zero (Firing et al., 1983). The potential implications of these anomalies are discussed in section 4.

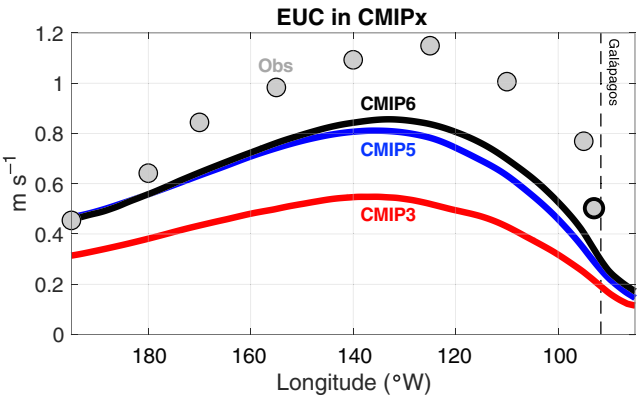

Figure 1. Peak EUC velocity (m s^{-1}) along the equatorial Pacific Ocean averaged across all CMIP3 models (red), CMIP5 models (blue), and CMIP6 models (black). Observations of Johnson et al. (2002) are indicated in gray circles with thin outlines, and the observations by ROGER are indicated by a gray circle with a thick outline at 93°W. The dashed line at 91.7°W marks the westernmost shoreline of the Galápagos Archipelago. See Figure S1 for all profiles from each CMIP.

3. Results With Discussion

3.1. A Broad View of the Equatorial Pacific

Before a direct comparison between GCM simulations and glider observations in the eastern Pacific, it is useful to contextualize EUC biases at the basin scale. As shown previously by Karnauskas et al. (2012), the CMIP3 multimodel mean severely underestimates the peak EUC velocity across the entire basin (Figure 1 and Figure S1 in the supporting information). In the central Pacific near 125°W, where the observed EUC is strongest, the CMIP3 multimodel mean peaks at 0.55 m s^{-1} compared to the observed value of 1.15 m s^{-1}. Both the CMIP5 and CMIP6 multimodel ensembles demonstrate impressive improvement over CMIP3. The peak EUC velocity in CMIP5 (CMIP6) is 47% (56%) faster than in CMIP3, and the slow bias is eliminated entirely west of the dateline. Despite these marked improvements, the peak EUC velocity in CMIP6 is still 33% slower than the observational estimate.

The rate of shoaling of the EUC across the Pacific, which is important for the development of the cold tongue, was also examined. The observed rate of EUC shoaling, estimated by linear regression between 165°E and 95°W, is 1.36 m per degree longitude (Johnson et al., 2002). Across the three CMIPs, there is again evidence of improvement—the multimodel mean of this metric is 75%, 79%, and 88% of the observed estimate in CMIP3, CMIP5, and CMIP6, respectively (Figure S2). It is reasonable that progress in simulating the slope of the EUC, closely associated with that of the thermocline, is coincident with progress in simulating its peak velocity. This coincidence only applies to the three CMIPs as a whole—there is no correlation across models *within* a CMIP between the slope and peak velocity of the EUC.

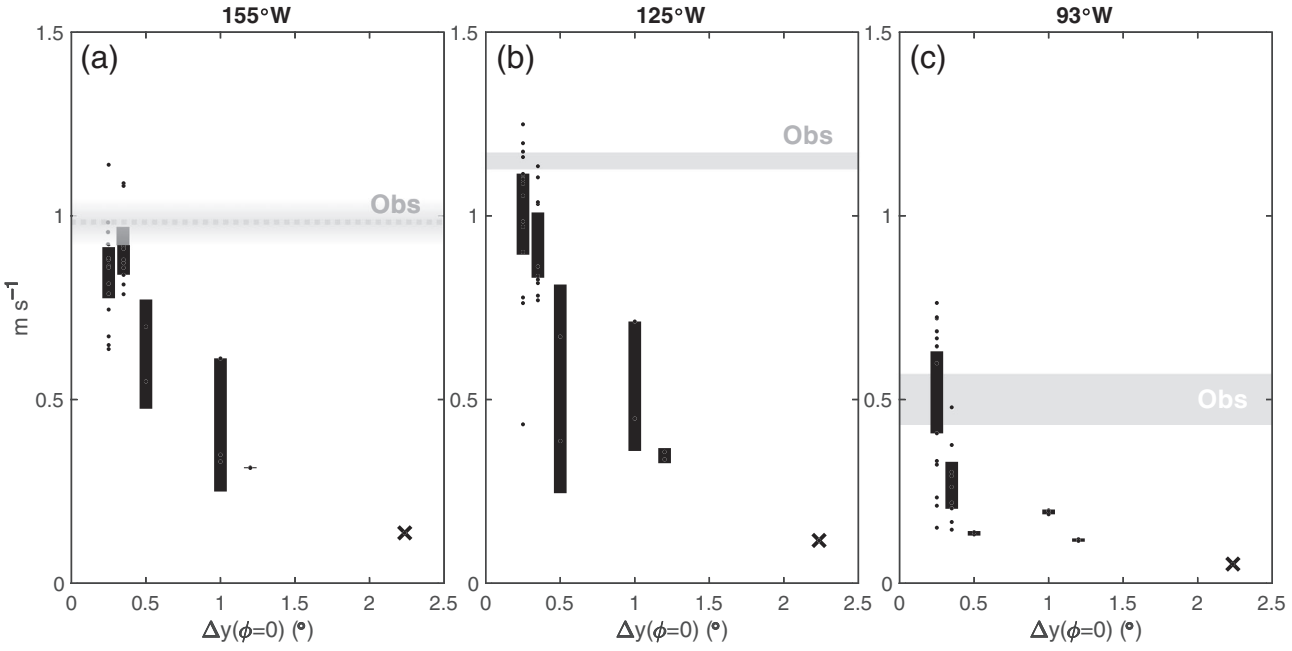

Figure 2. Peak EUC velocity (m s^{-1}) as a function of equatorial meridional resolution (degrees latitude) of the ocean component of CMIP6 models at three exemplar longitudes (155°W [a], 125°W [b], and 93°W [c]). The height of each black bar represents the mean peak EUC velocity from models within that resolution bin ± 2 standard errors. The X represents the (single) model with equatorial meridional resolution >2°. The observed peak EUC velocity is indicated by gray bars in each panel (155°W and 125°W from Johnson et al., 2002, and 93°W from ROGER), where the width of each bar is equivalent to the estimated observational uncertainty except for 155°W where only the mean value is presently available.

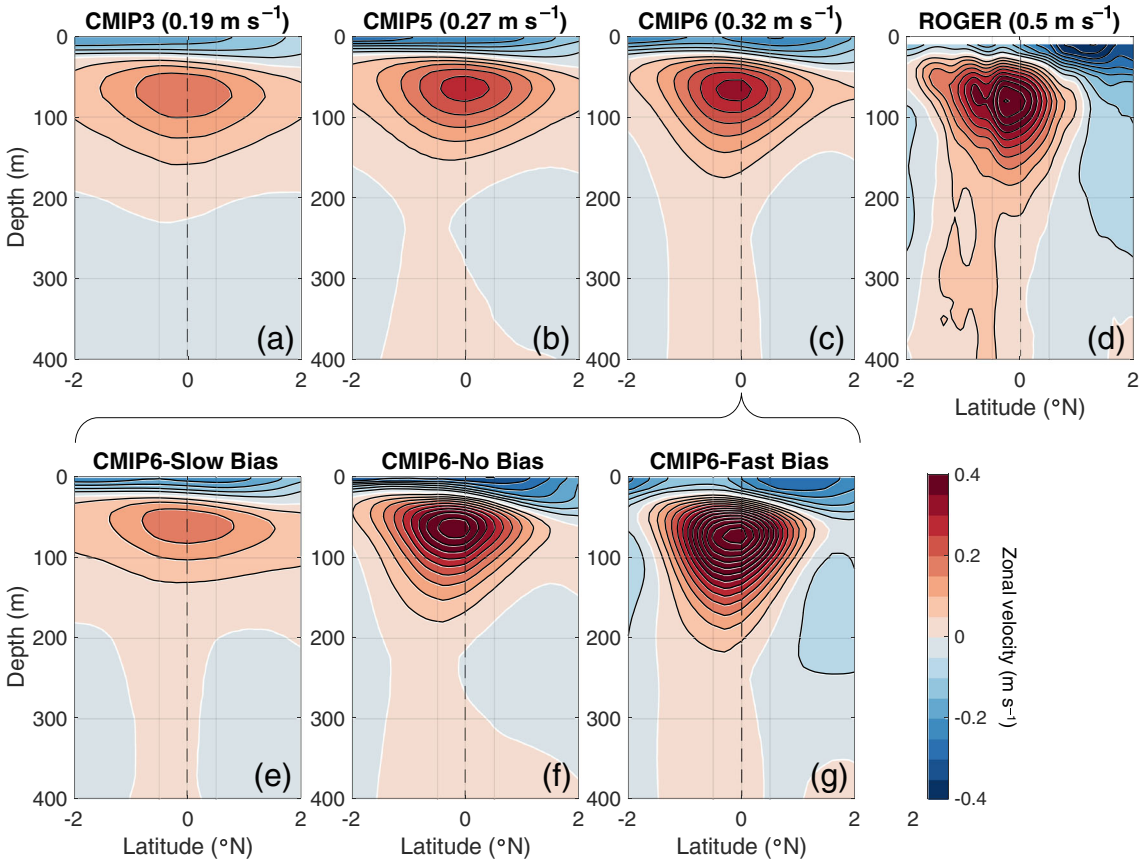

Figure 3. Mean zonal velocity (m s^{-1}) along 93°W averaged across all CMIP3 models (a), CMIP5 models (b), CMIP6 models (c), and the observations by ROGER (d). Contour interval 0.05 m s^{-1} with 0 m s^{-1} denoted by the white line. The maximum eastward velocity is indicated in the titles of panels (a)–(d). (e–g) As in (c) but averaged across subsets of CMIP6 models with a slow bias, negligible bias (within 0.1 m s^{-1} of ROGER), and fast bias. Latitude 0.5°S and 0.5°N grid lines are included on each panel, denoting the averaging interval used in Figure 4.

However, the strong dependence of peak EUC velocity on model resolution found for CMIP3 in Karnauskas et al. (2012) persists through CMIP6 (Figure 2). In particular, the meridional resolution near the equator of the ocean component of a GCM is a good predictor of simulated EUC velocity in CMIP6, especially in the eastern Pacific, where even the difference between the means of models with 0.25° and 0.33° resolution is statistically significant. An equatorial ocean meridional resolution of about 0.33° still appears necessary (albeit not always sufficient) to obtain the observed peak EUC velocity. These results are consistent with a recent study by Kuntz and Schrag (2020), who focused on the slow EUC bias in the central Pacific in CMIP5 models, and indicated that resolution and diffusivity parameterizations are contributing factors.

3.2. Assessment in the Eastern Pacific

The multimodel mean zonal velocity sections at 93°W from all three CMIPs (Figures 3a–3c) present a clearly identifiable EUC, with a core south of the equator in CMIP6. Above the EUC lies the westward South Equatorial Current (SEC), which is biased differently across the CMIPs and is described at the end of section 3.2. Similar to the GCM biases in peak EUC velocity across the Pacific, the EUC at 93°W is slower than observations (Figure 3d). Although there is clear improvement across the CMIPs (peak speeds increased from 0.19 m s^{-1} in CMIP3 to 0.32 m s^{-1} in CMIP6), the EUC in most of the individual GCMs is substantially slower than the observed peak EUC velocity observed by ROGER at 93°W of 0.50 m s^{-1}.

Examining the simulated and observed vertical structure of zonal velocity at 93°W (Figures 3a–3d and 4), the velocity profile above the EUC (down to ~50 m) is well simulated by CMIP5 and CMIP6, including a reasonable bulk vertical shear $\partial u/\partial z$. However, we find several discrepancies between the models and

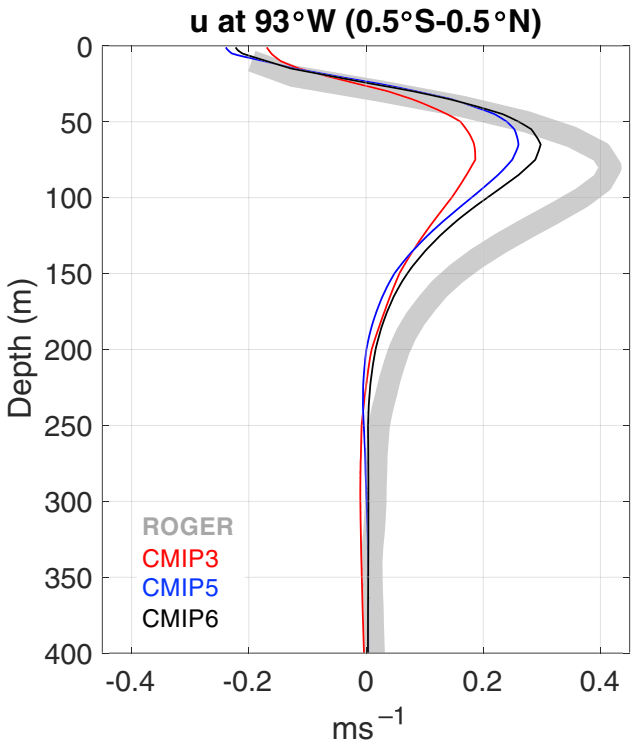

Figure 4. Vertical profile of zonal velocity (m s^{-1}) at 93°W averaged between 0.5°S and 0.5°N in ROGER observations (thick gray), CMIP3 (red), CMIP5 (blue), and CMIP6 (black).

observations above, within, and below the EUC. The simulated EUC core from 50–100 m is both too shallow and too weak. A weak EUC leads to a weak $\partial u/\partial z$ beneath the core. The weak bias of N^2 at and below the EUC core (Figure 5) is consistent with a weak bias of $\partial u/\partial z$ from consideration of the Richardson number. Above the EUC, vertical stratification in the CMIP6 multimodel mean is too strong from 2°S to 1°N and too weak near the equatorial front between 1°N and 2°N. The latter stratification biases are readily attributable to biases in potential temperature and salinity (Figure 6); the strong N^2 bias south of 1°N is caused by too much temperature stratification, and the weak N^2 bias north of 1°N is caused by too little salinity stratification. Indeed, the salinity fields at 93°W differ quite substantially between CMIP6 and ROGER, such that the fresh pool north of the equatorial front is not captured well, resulting in weak stratification in both the vertical and horizontal (Figure 6). It is possible that the strong stratification bias above the EUC is partially explained by the weak shear implied by the EUC core being too weak, but at the equatorial front, both vertical stratification and horizontal shear between the EUC and SEC are weak. A number of possible explanations for the latter result are possible, including models not raining enough over the warm/fresh pool north of the equatorial front or horizontal eddy diffusion being too strong in that location.

As was discussed in Karnauskas et al. (2012), velocity is an important metric for ocean dynamics, including tracer and momentum advection, vorticity, and mixing, but metrics based on peak velocity may overlook models whose diffusivity is high enough to compensate for coarse resolution to achieve a reasonable basin-scale mass balance. Indeed, simulated mean eastward transports through 93°W associated with the EUC (mean EUC transports calculated by integrating all eastward zonal velocity ($u > 0$) along 93°W from the surface to 250 m and from 2°S to 2°N.) are somewhat less biased relative to observations than velocities are—5.5, 6.3, and 6.4 Sv in CMIP3, CMIP5, and CMIP6, respectively, compared to 8.4 Sv from ROGER. This implies that the simulated EUC has a greater cross-sectional area, which is clearly evident in terms of width (Figures 3a–3d) and thus underscores the importance of horizontal

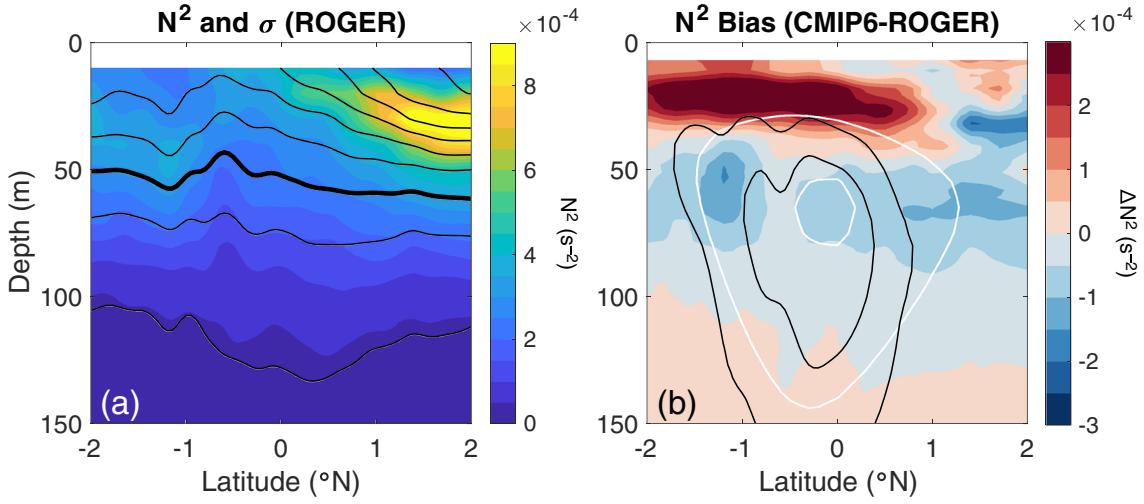

Figure 5. Mean buoyancy frequency squared (N^2, s^{-2}, shading) and potential density (σ, kg m^{-3}, black contours every 0.5 kg m^{-3} with 25 kg m^{-3} denoted by the thick line) along 93°W from ROGER (a). Difference between CMIP6 multimodel mean N^2 along 93°W and ROGER observations (b). For reference to the EUC, the zonal velocity is contoured in panel (b) at 0.1 and 0.3 m s^{-1} from the CMIP6 multimodel mean (white) and ROGER (black).

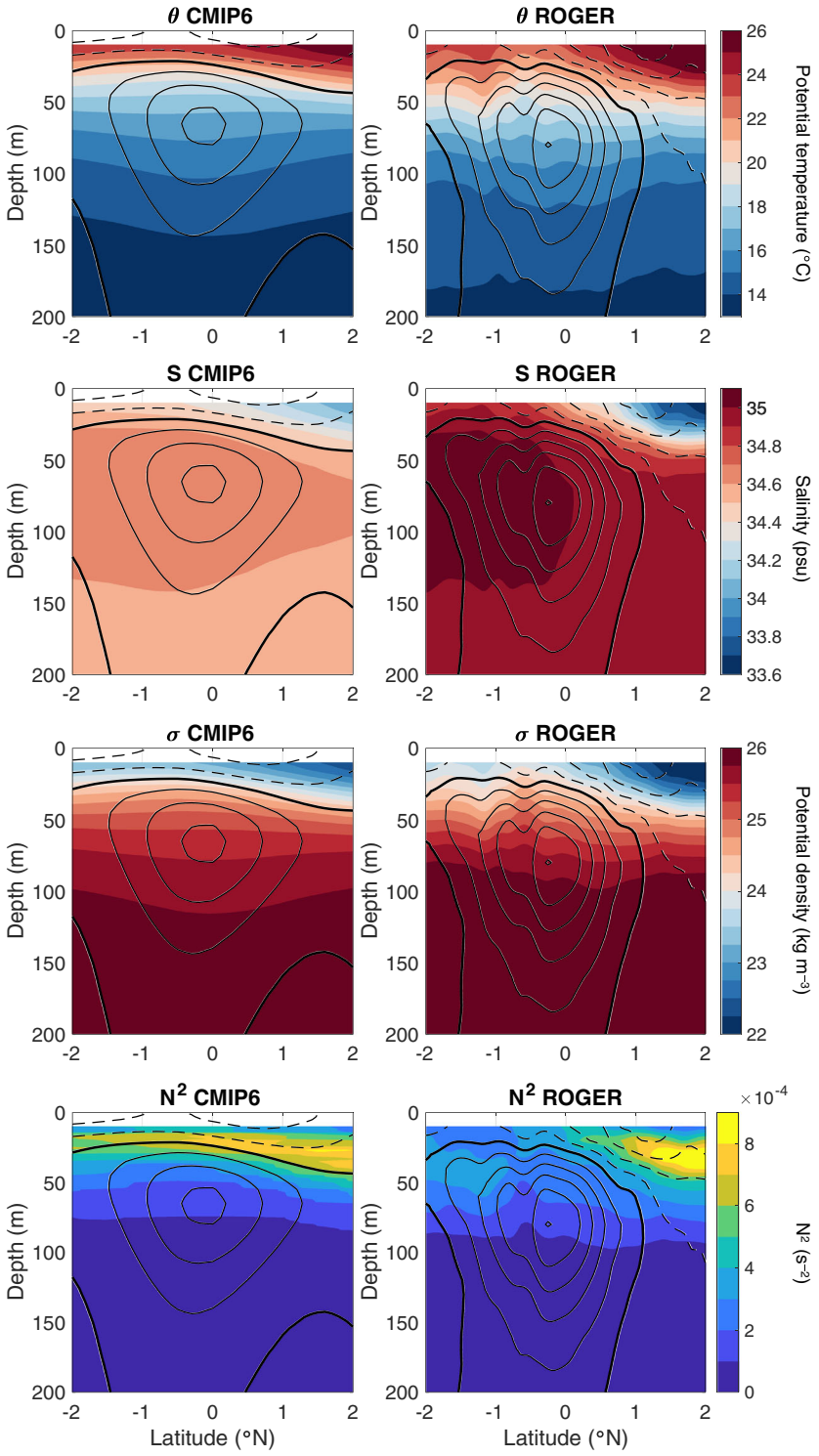

Figure 6. Cross sections of potential temperature (°C), salinity (psu), potential density (kg m^{-3}), and buoyancy frequency squared (N^2, s^{-2}) along 93°W in the CMIP6 multimodel mean (left column) and ROGER observations (right column). For reference to the EUC, contours of zonal velocity are overlaid upon the corresponding fields (interval 0.1 m s^{-1}).

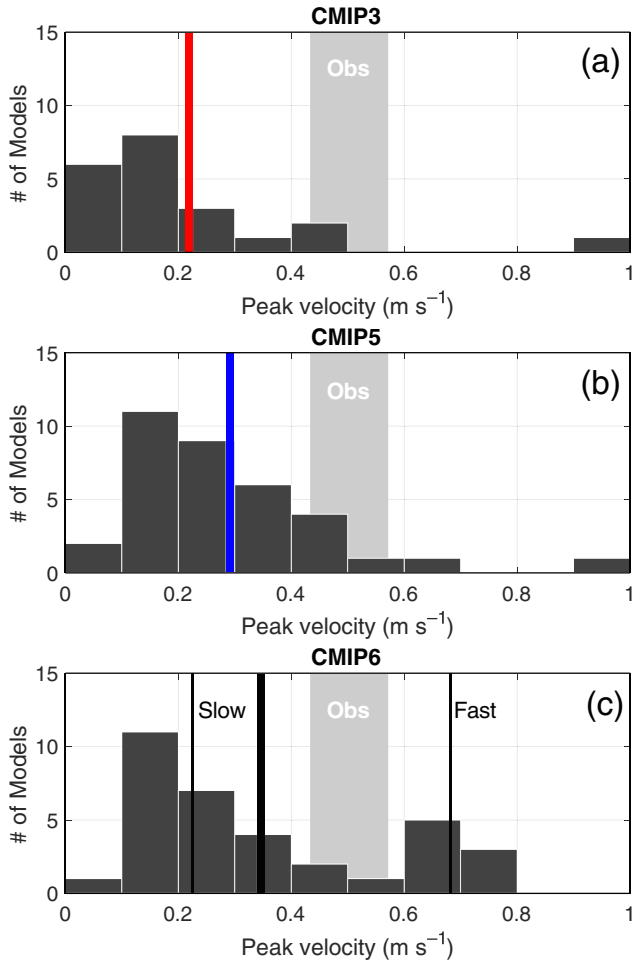

Figure 7. Histograms of peak EUC velocity (m s^{-1}) at 93°W in CMIP3 models (a), CMIP5 models (b), and CMIP6 models (c). Observations by ROGER are indicated by the gray bar (width ± 0.07 m s^{-1}). In each panel, the multimodel mean is indicated by a vertical line. In the CMIP6 panel, the multimodel means for subsets of models with slow and fast biases are also indicated by thin black lines.

viscosity. Finally, a curious feature that emerges only in CMIP5 and CMIP6 that compares well with ROGER observations is a very weak positive zonal velocity extending from the bottom of the EUC to beyond 400-m depth and centered near 0.5°S. This flow was present in Lukas (1986) and Kessler (2006) and considered part of the EUC; its structure, dynamics, and variability warrant further investigation.

The distribution of peak EUC velocity simulated by GCMs within a given CMIP has changed. In CMIP3 and CMIP5 (Figures 7a and 7b), there was a clear tendency for models to underestimate the strength of the EUC, well characterized by the multimodel means. In CMIP6 (Figure 7c), the distribution of the 34 GCMs is bimodal; 23 models have a slow bias (slower than ROGER by more than 0.1 m s^{-1}), only three models have a negligible bias (within 0.1 m s^{-1} of ROGER), and eight models have a *fast* bias (faster than the ROGER value by more than 0.1 m s^{-1}). Based on CMIP3 models, Karnauskas et al. (2012) proposed that slow EUC biases may be a result of nonlinear terms in the zonal momentum budget not being adequately resolved in coarse ocean grids (Brown et al., 2007; Kessler et al., 2003; Maes et al., 1997; Wacongne, 1990). While it is true that all eight CMIP6 models with an equatorial ocean meridional resolution of 0.5° or coarser have a slow bias and all eight CMIP6 models with a fast bias have an equatorial ocean meridional resolution of about 0.25°, resolution alone does not explain the bimodal distribution in CMIP6—in fact, many of the relatively high resolution (0.25–0.33°) CMIP6 models have a slow bias (Figure 2). As an integral part of the coupled system in the tropical Pacific, EUC biases may be linked to other mean state biases in both the ocean and atmosphere, including the Walker cell and the basin-scale thermocline tilt.

The bimodal distribution of peak EUC velocity simulated by CMIP6 models motivates a reexamination of the EUC structure, conditioned on their bias as defined above. Interestingly, the mean of the 23 CMIP6 models with a slow bias (Figure 3e) is very similar to the mean of all CMIP3 models (Figure 3a), save for the weak positive zonal velocity extending to 400 m. The peak EUC velocities are within about 0.1 m s^{-1} of each other, and neither exhibits the southward-shifted EUC core that is well resolved by ROGER, clear in the Johnson et al. (2002) climatology, and has been well understood for some time (Charney & Spiegel, 1971; Kessler et al., 1998; Philander & Delecluse, 1983). The similarity between the slow-biased CMIP6 models and the CMIP3 ensemble also includes their greater (especially wider) cross-sectional area so as to maintain a more realistic total volume transport, which narrows progressively with the nonbiased and fast-biased CMIP6 models similar to the narrowing from CMIP3 to CMIP6. The outstanding feature of the CMIP6 models with a fast EUC bias (Figure 3g) is not the EUC but the structure of the SEC. Particularly, the westward deep lobe of the SEC in the Northern Hemisphere evident in ROGER (and Johnson et al., 2002 at 110°W and 95°W) is only present in the CMIP6 models with a fast bias (Figures 3g and 8). The associated meridional shear of zonal velocity $\partial u/\partial y$ is very weak in CMIP3 and CMIP5 and slow-biased and even unbiased CMIP6 models, but $\partial u/\partial y$ for u averaged between 50 and 250 m in the Northern Hemisphere is remarkably well captured by the fast-biased CMIP6 models (Figure 8). Again, the difficulty in properly simulating the shear between the EUC and SEC appears relevant to stratification biases near the equatorial front via barotropic instability (Figure 5).

3.3. Encounter With the Galápagos

As mentioned in section 1, the encounter of the EUC with the Galápagos has important implications for regional ocean circulation and ecosystems, and modeling studies have demonstrated that it may even have consequences for basin-scale climate. The implementation of islands in an ocean model varies considerably

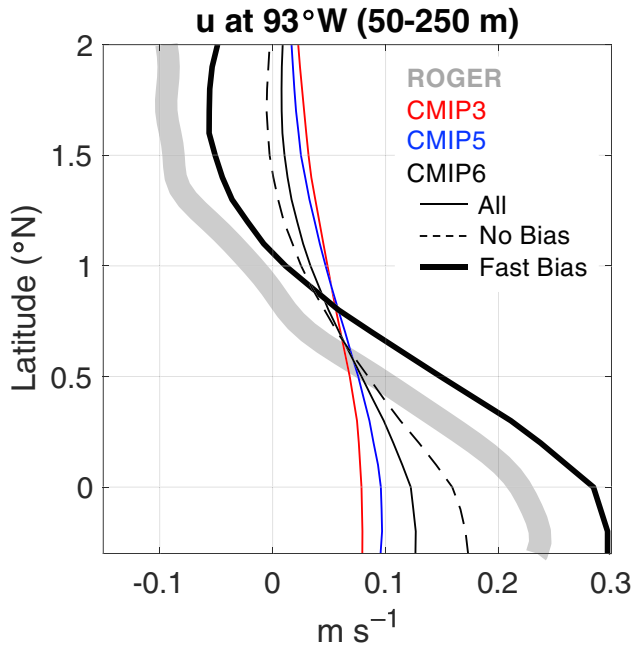

Figure 8. Meridional profiles of zonal velocity (m s^{-1}) along 93°W, averaged from 50–200 m in ROGER observations (thick gray), CMIP3 (red), CMIP5 (blue), and CMIP6 (black). Additionally, profiles for subsets of CMIP6 models with no bias (within 0.1 m s^{-1} of ROGER) and a fast bias are indicated with dashed and thick black lines, respectively.

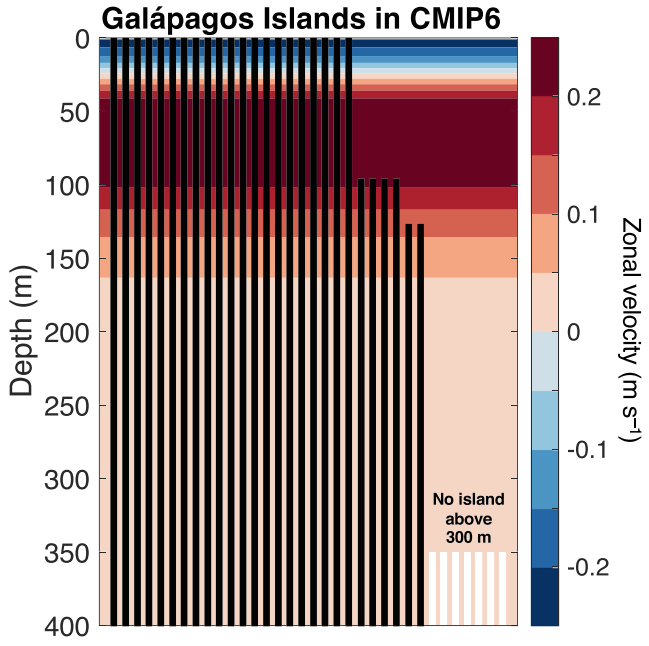

Figure 9. Illustration of the minimum depth of islands or seamounts representing the Galápagos Archipelago in CMIP6 models. The contoured field in the background is the CMIP6 multimodel mean zonal velocity (m s^{-1}) at 93°W, averaged between 0.5°S and 0.5°N. Contour interval 0.05 m s^{-1}.

between GCMs, generally beginning with a collection of grid points in the land-ocean mask designated as land with no-slip (and zero normal flow) lateral boundary conditions. Jakoboski et al. (2020) used a subset of ROGER observations to validate such model simulations, confirming that the islands induce a roughly even bifurcation of the EUC core (north and south of Isla Isabela) and a substantial upwelling rate based on net horizontal transport divergence. In CMIP3, few models had an ocean resolution high enough to give the archipelago more than one land-masked grid cell. Even when realistic and highly resolved bathymetry is used in an ocean model, that is only a starting point; in practice, sharp bathymetry is typically smoothed multiple times prior to integration to avoid numerical instability. This process can quickly render the Galápagos Islands a mere seamount in a GCM. As pointed out by Karnauskas et al. (2012), this was not of immediate consequence in CMIP3 models because the EUC was far too weak in the eastern Pacific, but it was cautioned that this may require careful attention when computing power becomes greater and ocean models are structured with higher resolution.

The generally higher resolution of ocean models in CMIP6 GCMs has finally afforded the Galápagos a nontrivial representation. Of the 34 CMIP6 models considered in this study, 21 have a "Galápagos" island reaching the surface, 6 have a seamount that terminates somewhere in the deep half of the EUC, and 7 have no island or seamount in the eastern equatorial Pacific Ocean above 300 m (Figure 9). A sampling of CMIP6 models with islands and their mean zonal velocity at the depth of the EUC core in the eastern equatorial Pacific is provided in Figure 10. These model islands effectively represent Isla Isabela (the largest and one of the westernmost islands in the archipelago, spanning 1.06°S to 0.17°N in reality). Comparison of two of the three models without an EUC bias at 93°W (Figures 10a and 10b; the third such model has a seamount terminating at 200 m) reveals something that may seem excessively minor but is responsible for a large difference in the eventual termination of the EUC: whether or not the island crosses (or even reaches) the equator matters. In the case of the model with an island that does not quite reach the equator (Figure 10a), the EUC is only partially blocked and easily flows around the north side of the island—quite at odds with observational studies from Lukas (1986) to Jakoboski et al. (2020). Such a circulation would clearly have implications for the distribution of upwelling throughout the region from west of the Galápagos to the coast of Peru and for the marine and terrestrial biogeography of the Galápagos Archipelago (Boersma et al., 2013; Houvenaghel, 1978; Karnauskas et al., 2015). In the second unbiased model, whose island just reaches the equator (Figure 10b), the EUC bifurcation is roughly even between north and south, despite the island itself being much more substantial in the Southern Hemisphere—keep in mind that the EUC, too, is centered south of the equator due to the cross-equatorial component of the trade winds in the eastern Pacific. Finally, two models with very different simulations of the EUC (slow and fast biased) yet effectively similar representations of the Galápagos (Figures 10c and 10d) yield reasonable reproductions of the EUC bifurcation seen in ROGER observations (Jakoboski et al., 2020) and previous OGCM simulations at low (Karnauskas et al., 2007) and high (Karnauskas et al., 2014) resolution that adequately represent the Galápagos. In the lower resolution CMIP6 model (Figure 10c), the absence of the island may be relatively inconsequential due to the slow bias, but in

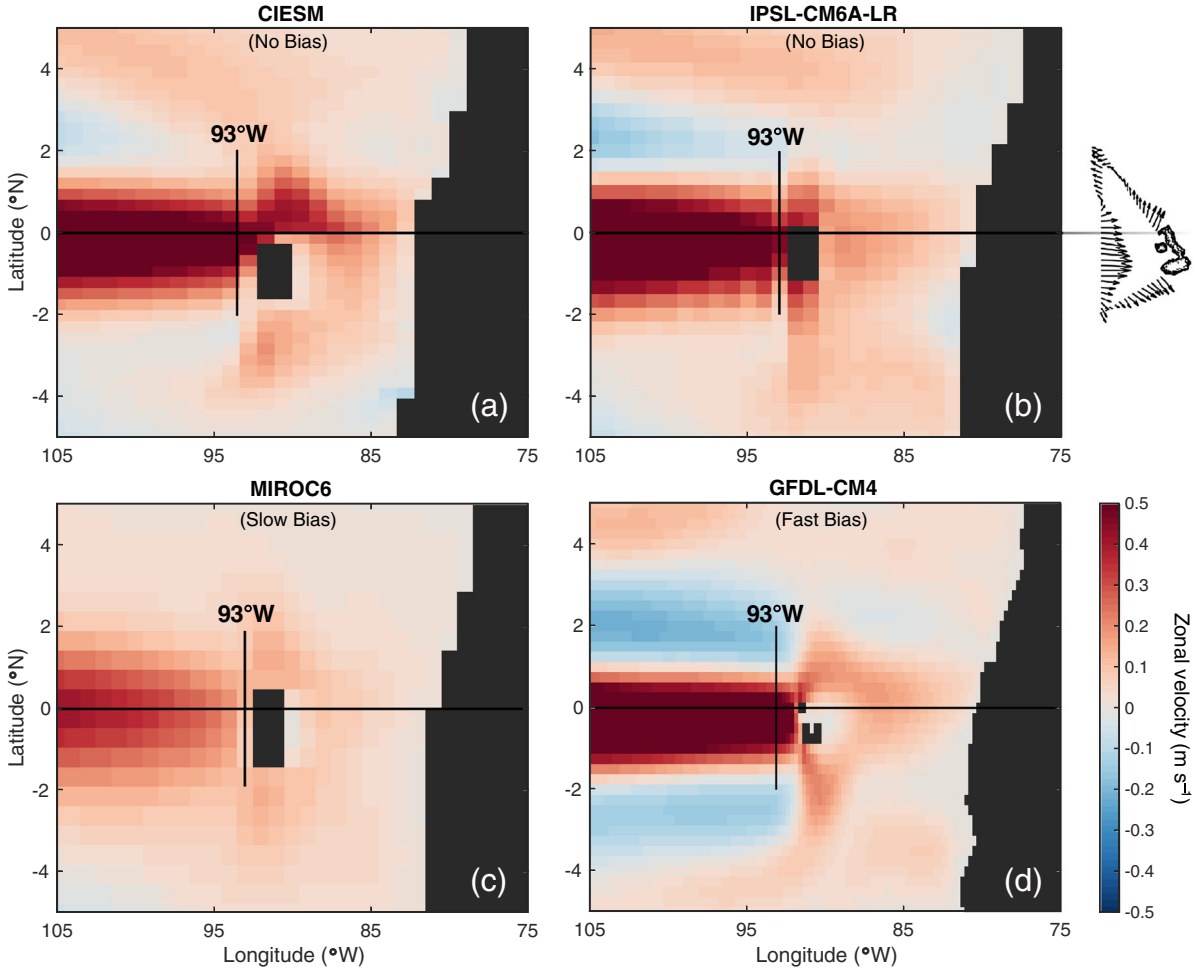

Figure 10. Plan view of zonal velocity (m s^{-1}) in the eastern equatorial Pacific Ocean on the native grids of four exemplar CMIP6 models: the Community Integrated Earth System Model (CIESM) from Tsinghua University (Lin et al., 2019), the Institut Pierre-Simon Laplace (IPSL) Climate Model version 6A-Low Resolution (CM6A-LR; Boucher et al., 2020), the Model for Interdisciplinary Research on Climate version 6 (MIROC6; Tatebe et al., 2019), and the NOAA/Geophysical Fluid Dynamics Laboratory (GFDL) Coupled Model version 4 (CM4; Held et al., 2019). The depth presented is that of the peak EUC velocity at 93°W, which varies slightly from model to model between 60 and 80 m. The locations of the 93°W section from ROGER and the equator are indicated by black lines. To the right of the top row of the figure is a simplified (but appropriately scaled) reproduction of Figure 10b of Jakoboski et al. (2020), illustrating the time-mean currents averaged over 35–75 m during the ROGER campaign.

higher resolution GCMs with a fast bias (Figure 10d), it is quite apparent that adequately representing the Galápagos at the equator is crucial. Interestingly, the presence of a small gap (one ocean grid cell wide) between individual islands near the equator (Figure 10d) does not permit eastward flow—likely a consequence of a no-slip boundary condition along the sidewalls of islands. An island configuration reaching, extending beyond, or even straddling the equator is the chief criterion for obtaining an adequate termination of the EUC.

4. Summary and Conclusion

We have examined the representation of the Pacific EUC in 90 coupled models across three generations (CMIP3, CMIP5, and CMIP6), with a special focus on the eastern Pacific and the EUC's encounter with the Galápagos Islands. We found a marked improvement in the simulation of the EUC in each CMIP generation, although the simulated EUC remains weak on average and its peak velocity at all longitudes still exhibits a dependence on ocean model resolution. A major El Niño in 2015–2016 occurred within the 3 years of ROGER observations along 93°W. During El Niño events, the EUC weakens and may introduce a slow bias into the time mean (Firing et al., 1983), which suggests these GCM biases may be understated in our

model-data comparison. Analyses of shear and stratification indicate that the weak EUC bias and the absence of a deep lobe of the SEC to its north likely have implications for mixing in both the horizontal and vertical and therefore may be a culprit in systematic GCM biases within the cold tongue and along the equatorial front. A census of the model islands representing the Galápagos in the CMIP6 ensemble indicates that roughly two thirds of them represent the Galápagos, but not always adequately. Ocean model grids should include an island crossing the equator, especially if the model simulates a realistic (or too strong) EUC. This may be something of a self-correcting problem, as higher horizontal resolution appears to result in a faster EUC *and* would automatically facilitate the survival of small islands upon smoothing real bathymetry, but care must be taken that those islands adequately reach the equator to avoid a host of new biases such as between the Galápagos and mainland South America.

Data Availability Statement

All CMIP3, CMIP5, and CMIP6 model outputs were acquired from the Earth System Grid Federation (ESGF, https://esgf-node.llnl.gov). The spatially reduced and regridded time mean CMIPx fields described in section 2.1 are available at https://scholar.colorado.edu/concern/datasets/f1881n01t and may be cited using the following https://doi.org/10.25810/pk4z-n050 (Karnauskas, 2020). Spray glider observations from ROGER are available at http://spraydata.ucsd.edu and should be cited using the following https://doi.org/10.21238/S8SPRAY0090 (Rudnick, Owens, Karnauskas, et al., 2020). Equatorial Pacific mean zonal velocity fields are available at https://floats.pmel.noaa.gov/gregory-c-johnson-home-page (Johnson et al., 2002).

Acknowledgments

We thank Sonya Legg and Frank Bryan for helpful discussions about ocean models and Gregory Johnson about observations. We also thank three anonymous reviewers and Editor Lei Zhou for their constructive comments to improve the manuscript and Andrew Johnson for generous assistance with data archival. We gratefully acknowledge support from the National Science Foundation (OCE-1232971 and OCE-1233282) and the Global Ocean Monitoring and Observing program (formerly the Ocean Observing and Monitoring Division) of the National Oceanographic and Atmospheric Administration (NA13OAR4830216). Glider operations were expertly conducted by personnel at the Instrument Development Group at the Scripps Institution of Oceanography and by the glider operations group at Woods Hole Oceanographic Institution. We appreciate the tremendous support of the Ecuadorian Instituto Oceanográfico de la Armada (INOCAR) during glider operations. We acknowledge the Program for Climate Model Diagnosis and Intercomparison and the World Climate Research Programme, which, through its Working Group on Coupled Modelling, coordinated and promoted CMIP3, CMIP5, and CMIP6. We thank the climate modeling groups for producing and making available their model output, the Earth System Grid Federation (ESGF) for archiving the data and providing access, and the multiple funding agencies that support CMIP efforts and the ESGF.

References

Bjerknes, J. (1969). Atmospheric teleconnections from the equatorial Pacific. *Monthly Weather Review*, *97*, 163–172.

Boersma, P. D., Steinfurth, A., Merlen, G., Jiménez-Uzcátegui, G., Vargas, F., & Parker, P. G. (2013). Galápagos Penguin (*Spheniscus mendiculus*). In P. G. Borboroglu & P. D. Boersma (Eds.), *Penguins natural history and conservation* (pp. 1–360). Seattle, WA: University of Washington Press. Retrieved from http://www.washington.edu/uwpress/search/books/BORPEN.html

Boucher, O., Servonnat, J., Albright, A. L., Aumont, O., Balkanski, Y., Bastrikov, V., et al. (2020). Presentation and evaluation of the IPSL-CM6A-LR climate model. *Journal of Advances in Modeling Earth Systems*, *12*, e2019MS002010. https://doi.org/10.1029/2019MS002010

Brown, J. N., Godfrey, J. S., & Fiedler, R. (2007). A zonal momentum balance on density layers for the central and eastern equatorial Pacific. *Journal of Physical Oceanography*, *37*, 1939–1955.

Bryden, H. L., & Brady, E. C. (1985). Diagnostic model of three-dimensional circulation in the upper equatorial Pacific Ocean. *Journal of Physical Oceanography*, *15*, 1255–1273.

Busecke, J. J. M., Resplandy, L., & Dunne, J. P. P. (2019). The Equatorial Undercurrent and the oxygen minimum zone in the Pacific. *Geophysical Research Letters*, *46*, 6716–6725. https://doi.org/10.1029/2019GL082692

Charney, J. G., & Spiegel, S. L. (1971). The structure of wind-driven equatorial currents in homogeneous oceans. *Journal of Physical Oceanography*, *1*, 149–160.

Coats, S., & Karnauskas, K. B. (2018). A role for the Equatorial Undercurrent in the ocean dynamical thermostat. *Journal of Climate*, *31*, 6245–6261.

Cravatte, S., Madec, G., Izumo, T., Menkes, C., & Bozec, A. (2007). Progress in the 3-D circulation of the eastern equatorial Pacific in a climate ocean model. *Ocean Modelling*, *17*, 28–48.

Doney, S. C., & Karnauskas, K. B. (2014). Oxygen and climate dynamics. *Nature Climate Change*, *4*(10), 862–863. https://doi.org/10.1038/nclimate2386

Drenkard, E. J., & Karnauskas, K. B. (2014). Strengthening of the Pacific Equatorial Undercurrent in the SODA ocean reanalysis: Mechanisms, ocean dynamics, and implications. *Journal of Climate*, *27*, 2405–2416.

Eden, C., & Timmermann, A. (2004). The influence of the Galápagos Islands on tropical temperatures, currents and the generation of tropical instability waves. *Geophysical Research Letters*, *31*, L15308. https://doi.org/10.1029/2004GL020060

Eyring, V., Bony, S., Meehl, G. A., Senior, C. A., Stevens, B., Stouffer, R. J., & Taylor, K. E. (2016). Overview of the Coupled Model Intercomparison Project Phase 6 (CMIP6) experimental design and organization. *Geoscientific Model Development*, *9*, 1937–1958.

Feely, R. A., Boutin, J., Cosca, C. E., Dandonneau, Y., Etcheto, J., Inoue, H. Y., et al. (2002). Seasonal and interannual variability of CO_2 in the equatorial Pacific. *Deep-Sea Research Part II*, *49*(13–14), 2443–2469. https://doi.org/10.1016/S0967-0645(02)00044-9

Feldman, G., Clark, D., & Halpern, D. (1984). Satellite ocean color observations of the phytoplankton distribution in the eastern equatorial Pacific during the 1982–1983 El Niño. *Science*, *226*(4678), 1069–1071. https://doi.org/10.1126/science.226.4678.1069

Firing, E., Lukas, R., Sadler, J., & Wyrtki, K. (1983). Equatorial Undercurrent disappears during 1982–1983 El Niño. *Science*, *222*(4628), 1121–1123. https://doi.org/10.1126/science.222.4628.1121

Hayashi, M., Jin, F.-F., & Stuecker, M. F. (2020). Dynamics for El Niño-La Niña asymmetry constrain equatorial-Pacific warming pattern. *Nature Communications*, *11*(1). https://doi.org/10.1038/s41467-020-17983-y

Held, I. M., Guo, H., Adcroft, A., Dunne, J. P., Horowitz, L. W., Krasting, J., et al. (2019). Structure and performance of GFDL's CM4.0 climate model. *Journal of Advances in Modeling Earth Systems*, *11*, 3691–3727. https://doi.org/10.1029/2019MS001829

Houvenaghel, G. T. (1978). Oceanographic conditions in the Galapagos archipelago and their relationships with life on the islands. In R. Boje & M. Tomczak (Eds.), *Upwelling ecosystems* (Chapter 15, pp. 181–200). Berlin, Heidelberg: Springer.

Jakoboski, J., Todd, R. E., Owens, W. B., Karnauskas, K. B., & Rudnick, D. L. (2020). Bifurcation and upwelling of the Equatorial Undercurrent west of the Galápagos Archipelago. *Journal of Physical Oceanography*, *50*, 887–905.

Johnson, E. S., & Luther, D. S. (1994). Mean zonal momentum balance in the upper and central equatorial Pacific Ocean. *Journal of Geophysical Research*, *99*, 7689–7705.

Johnson, G. C., Sloyan, B. M., Kessler, W. S., & McTaggart, K. E. (2002). Direct measurements of upper ocean currents and water properties across the tropical Pacific Ocean during the 1990's. *Progress in Oceanography*, *52*, 31–61.
Karnauskas, K. B. (2020). Repeat Observations by Gliders in the Equatorial Region (ROGER) [Data set]. University of Colorado Boulder. https://doi.org/10.25810/PK4Z-N050
Karnauskas, K. B., & Cohen, A. L. (2012). Equatorial refuge amid tropical warming. *Nature Climate Change*, *2*(7), 530–534.
Karnauskas, K. B., Cohen, A. L., & Gove, J. M. (2016). Mitigation of coral reef warming across the central Pacific by the Equatorial Undercurrent: A past and future divide. *Scientific Reports*, *6*, 21213.
Karnauskas, K. B., Jenouvrier, S., Brown, C. W., & Murtugudde, R. (2015). Strong sea surface cooling in the eastern equatorial Pacific and implications for Galápagos penguin conservation. *Geophysical Research Letters*, *42*, 6432–6437. https://doi.org/10.1002/2015GL064456
Karnauskas, K. B., Johnson, G. C., & Murtugudde, R. (2012). An equatorial ocean bottleneck in global climate models. *Journal of Climate*, *25*, 343–349.
Karnauskas, K. B., Johnson, G. C., & Murtugudde, R. (2017). On the climate impacts of atolls in the central equatorial Pacific. *International Journal of Climatology*, *37*, 197–203.
Karnauskas, K. B., Murtugudde, R., & Busalacchi, A. J. (2007). The effect of the Galápagos Islands on the equatorial Pacific cold tongue. *Journal of Physical Oceanography*, *37*, 1266–1281.
Karnauskas, K. B., Murtugudde, R., & Busalacchi, A. J. (2010). Observing the Galápagos–EUC interaction: Insights and challenges. *Journal of Physical Oceanography*, *40*, 2768–2777.
Karnauskas, K. B., Murtugudde, R., & Owens, W. B. (2014). Climate and the global reach of the Galápagos Archipelago: State of the knowledge. In K. S. Harpp, E. Mittelstaedt, N. d'Ozouville, D. W. Graham (Eds.), *The Galápagos: A natural laboratory for the Earth sciences* (Chapter 11, pp. 215–231). Hoboken, New Jersey: John Wiley & Sons, Inc.
Kessler, W. S. (2006). The circulation of the eastern tropical Pacific: A review. *Progress in Oceanography*, *69*, 181–217.
Kessler, W. S., Johnson, G. C., & Moore, D. W. (2003). Sverdrup and nonlinear dynamics of the Pacific equatorial currents. *Journal of Physical Oceanography*, *33*, 994–1008.
Kessler, W. S., Rothstein, L. M., & Chen, D. K. (1998). The annual cycle of SST in the eastern tropical Pacific, diagnosed in an ocean GCM. *Journal of Climate*, *11*, 777–799.
Kuntz, L. B., & Schrag, D. P. (2020). Representation of the equatorial undercurrent in CMIP5 models. *Journal of Physical Oceanography*, *50*(10), 2997–3007. https://doi.org/10.1175/jpo-d-20-0007.1
Lin, Y.-L., Qin, Y., Xu, S., Huang, W., Xu, F., Liu, L., et al. (2019). The Community Integrated Earth System Model (CIESM) from Tsinghua University and its plan for CMIP6 experiments. *Climate Change Research*, *15*(5), 545–550.
Lukas, R. (1986). The termination of the Equatorial Undercurrent in the eastern Pacific. *Progress in Oceanography*, *16*, 63–90.
Luo, Y., Rothstein, L. M., & Zhang, R.-H. (2009). Response of Pacific subtropical-tropical thermocline water pathways and transports to global warming. *Geophysical Research Letters*, *36*, L04601. https://doi.org/10.1029/2008gl036705
Maes, C., Madec, G., & Delecluse, P. (1997). Sensitivity of an equatorial Pacific OGCM to the lateral diffusion. *Monthly Weather Review*, *125*, 958–971.
McPhaden, M. J., Busalacchi, A. J., Cheney, R., Donguy, J. R., Gage, K. S., Halpern, D., et al. (1998). The Tropical Ocean Global Atmosphere observing system: A decade of progress. *Journal of Geophysical Research*, *103*(C7), 14,169–14,240. https://doi.org/10.1029/97JC02906
Meehl, G. A., Covey, C., Delworth, T., Latif, M., McAvaney, B., Mitchell, J. F., et al. (2007). THE WCRP CMIP3 multimodel dataset: A new era in climate change research. *Bulletin of the American Meteorological Society*, *88*, 1383–1394.
Pedlosky, J. (1988). Entrainment and the termination of the Equatorial Undercurrent. *Journal of Physical Oceanography*, *18*, 880–886.
Philander, S. G. H., & Delecluse, P. (1983). Coastal currents in low latitudes (with application to the Somali and El Niño currents). *Deep Sea Research*, *30*, 887–902.
Qiao, L., & Weisberg, R. H. (1997). The zonal momentum balance of the Equatorial Undercurrent in the Central Pacific. *Journal of Physical Oceanography*, *27*, 1094–1119.
Rudnick, D. L. (2016). Ocean research enabled by underwater gliders. *Annual Review of Marine Science*, *8*, 519–541.
Rudnick, D. L., Davis, R. E., Eriksen, C. C., Fratantoni, D. M., & Perry, M. J. (2004). Underwater gliders for ocean research. *Marine Technology Society Journal*, *38*, 73–84.
Rudnick, D. L., Owens, W. B., Johnston, T. M. S., Karnauskas, K. B., Jakoboski, J., & Todd, R. E. (2020). The equatorial current system during the 2014–2016 El Niño as observed by underwater gliders. *Journal of Physical Oceanography*. https://doi.org/10.1175/JPO-D-20-0064.1
Rudnick, D. L., Owens, W. B., Karnauskas, K. B., & Johnston, T. M. S. (2020). Repeat observations by gliders in the equatorial region [Data set]. Scripps Institution of Oceanography, Instrument Development Group. https://doi.org/10.21238/S8SPRAY0090
Rudnick, D. L., Sherman, J. T., & Wu, A. P. (2018). Depth-average velocity from Spray underwater gliders. *Journal of Atmospheric and Oceanic Technology*, *35*, 1665–1673.
Sherman, J., Davis, R. E., Owens, W. B., & Valdes, J. (2001). The autonomous underwater glider "Spray". *IEEE Journal of Oceanic Engineering*, *26*, 437–446.
Sloyan, B. M., Johnson, G. C., & Kessler, W. S. (2003). The Pacific cold tongue: A pathway for interhemispheric exchange. *Journal of Physical Oceanography*, *33*, 1027–1043.
Tatebe, H., Ogura, T., Nitta, T., Komuro, Y., Ogochi, K., Takemura, T., et al. (2019). Description and basic evaluation of simulated mean state, internal variability, and climate sensitivity in MIROC6. *Geoscientific Model Development*, *12*(7), 2727–2765. https://doi.org/10.5194/gmd-12-2727-2019
Taylor, K. E., Stouffer, R. J., & Meehl, G. A. (2012). An overview of CMIP5 and the experiment design. *Bulletin of the American Meteorological Society*, *93*, 485–498.
Todd, R. E., Rudnick, D. L., Sherman, J. T., Owens, W. B., & George, L. (2017). Absolute velocity estimates from autonomous underwater gliders equipped with Doppler current profilers. *Journal of Atmospheric and Oceanic Technology*, *34*, 309–333.
Wacongne, S. (1990). On the difference in strength between Atlantic and Pacific undercurrents. *Journal of Physical Oceanography*, *20*, 792–799.
Warner, S. J., & Moum, J. N. (2019). Feedback of mixing to ENSO phase change. *Geophysical Research Letters*, *46*, 13,920–13,927. https://doi.org/10.1029/2019GL085415
Wyrtki, K. (1975). El Niño—The dynamic response of the equatorial Pacific Ocean to atmospheric forcing. *Journal of Physical Oceanography*, *5*(4), 572–584.
Yu, Z., & Schopf, P. S. (1997). Vertical eddy mixing in the tropical upper ocean: Its influence on zonal currents. *Journal of Physical Oceanography*, *27*, 1447–1458.